

NRL Report 7574

UNCLASSIFIED

# Determination of Ocean Surface Descriptors Using Sea Photo Analysis Techniques

R. O. PILON

*Aerospace Radar Branch  
Radar Division*

July 18, 1973



**NAVAL RESEARCH LABORATORY**  
Washington, D.C.

Approved for public release; distribution unlimited.

## CONTENTS

	Page
Abstract .....	ii
Problem Status .....	ii
Authorization .....	ii
INTRODUCTION .....	1
RECORDING SURFACE SLOPES .....	2
OPTICAL ANALYSIS .....	6
THE OCEAN SPECTRUM .....	9
COMPUTER ANALYSIS .....	14
MINOR SPECTRAL DISTORTIONS .....	15
DATA ANALYSIS .....	17
CONCLUSIONS .....	26
ACKNOWLEDGMENTS .....	29
REFERENCES .....	29
APPENDIX—Hindcast Data and Comparison with Inferred Descriptors .....	30

## ABSTRACT

The techniques of Sea Photo Analysis have been used to obtain surface truth descriptors of the open ocean from an aircraft. Aerial photographs were taken such that the density fluctuations of the negatives were related to surface slope. The slope spectra, obtained by Fourier analysis of the negatives, were fitted to an equivalent form of the Pierson-Moskowitz wave height spectrum. The photographs, the wave height spectrum, and the rms slope equations determined by Cox and Munk then yielded the averaged heading of the waves, the equivalent wind speed, the rms wave height, and the rms slope for clean and slick surfaces. The optical techniques of Sea Photo Analysis used in this program and digital analysis, used when whitecaps were present in the photographs, are discussed. The empirical equations used to determine rms wave height and slope and auxiliary rms slope and wave height spectrum equations are given. Surface descriptors were inferred for seas driven by winds from 3 to 21 knots occurring on 16 separate days.

## PROBLEM STATUS

This is the final report on the first phase of the NRL Problem

## AUTHORIZATION

NRL Problem R07-20  
Project FAA DOT-FA71WAI-220

Manuscript submitted March 13, 1973.

## DETERMINATION OF OCEAN SURFACE DESCRIPTORS USING SEA PHOTO ANALYSIS TECHNIQUES

### INTRODUCTION

The Naval Research Laboratory has been providing interpretation and quantitative analysis of aerial photography of the ocean surface, and related consultive assistance, to the Federal Aviation Administration, Department of Transportation. The analysis is being used by FAA in its study of multipath effects in communications between satellites and aircraft flying over the ocean. The techniques of Sea Photo Analysis [1], developed at NRL, have been used to obtain the ground truth descriptors of the ocean necessary in attempting to correlate multipath effects with the roughness of the scattering surface.

The ocean surface roughness may be described in terms of two components—sea and swell. Sea is the roughness generated by the local wind. Light winds ripple the ocean surface with short-wavelength, small-amplitude wavelets which decay rapidly. If the wind persists, the wavelets are constantly regenerated and longer wavelengths appear. As the wind increases and persists over a sufficiently large area, the proportion of the longer wavelength waves increases and the ocean becomes rougher. Therefore all wavelengths, with small probabilities of existence for the extremely long and short waves, constitute the roughness referred to as sea. Swell is the remnant of a sea generated in the area by a wind field that existed at some previous time or that propagated from a sea generated elsewhere, possibly thousands of miles away. As time passes since the wind field has died out or moved on, or as the swell system propagates out of a generating region, the short wavelengths disappear first, with the successively longer wavelengths decaying at slower rates. Thus swell commonly consists only of the long wavelengths generated by a wind.

The Naval Research Laboratory has been analyzing aerial photographs to determine the parameters describing the sea. This type of analysis is generally not applicable to swell but is limited to the relatively short wavelengths present in a sea by the clarity of the earth's atmosphere, the stability of airborne platforms, the quality of presently available optics, and the physical and chemical properties of photographic film. The FAA has been obtaining supplementary data on swell through hindcasts by the Naval Oceanographic Office (see the Appendix).

In Sea Photo Analysis (SPA) the physical processes by which the ocean surface is depicted in a negative are identified to yield the relationship between the surface parameters and the optical density of the negative. In the type of analysis used here the density is given in terms of the surface slope. When the photographic negative is optically analyzed, the intensity of the diffraction pattern is proportional to the slope spectrum of the ocean. The valid portion of the spectrum, which is restricted by the size of the area that can be photographed and the resolution of the photographic process, is fitted to an accepted form of the spectrum encompassing all wavelengths. The total slope spectrum together with other experimentally determined relationships, yield the surface descriptors.

The next three sections of this report are devoted to the mathematical basis of this type of analysis. The relationship between the density of the negative and the surface slopes of the ocean is developed, and it is shown that optical analysis yields the slope spectrum. A slope spectrum corresponding to the optical spectrum is derived from the Pierson-Moskowitz wave-height spectrum, and the empirical relationships used to determine the rms wave height and rms slope are given.

The theory is then extended to computer analysis of the photography, which had to be used in eight of the sixteen sets of data that could be analyzed. Next, minor distortions in the optical spectrum and ways to avoid them are described. Finally, the data and results of the data analysis are discussed.

### RECORDING SURFACE SLOPES

The local coordinate system used to develop the theoretical basis of the analysis is shown in Fig. 1. In this particular study the ocean was photographed from an aircraft

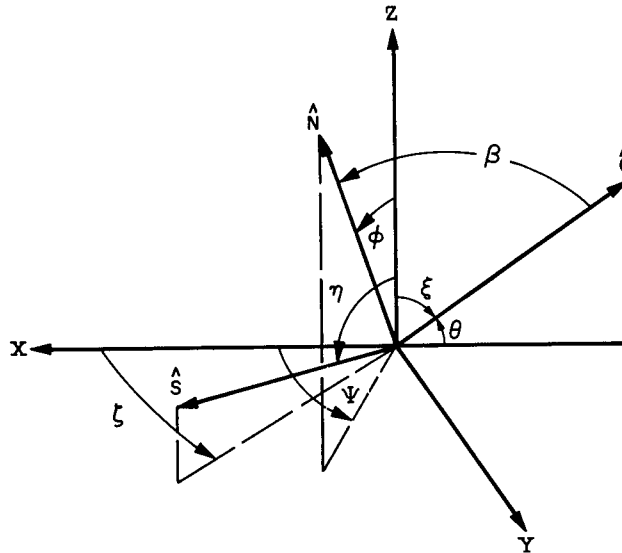


Fig. 1—The local coordinate system used in Sea Photo Analysis

flying in the minus-X direction, with a possible Y component dependent on analysis criteria. The camera was positioned such that its optical axis was pointing aft and downward at an angle of  $40^\circ$ . The position of the origin of the coordinate system shown in Fig. 1 is variable and located at the central point of the area being analyzed. In most of the analyses the aircraft would be flying directly in the minus-X direction with the unit vector  $\hat{C}$ , in the XZ plane, directed toward the camera. The variable in the location of the origin would then be the angle  $\theta$ , with  $\theta$  being equal to  $40^\circ$  in the center of the negative.

If a single sinusoid were propagating on the ocean surface at an angle  $\Psi$  with respect to the X axis, the local coordinate system would appear as shown in Fig. 2. At the origin the steepest gradient on the water surface makes an angle  $\phi$  with respect to the

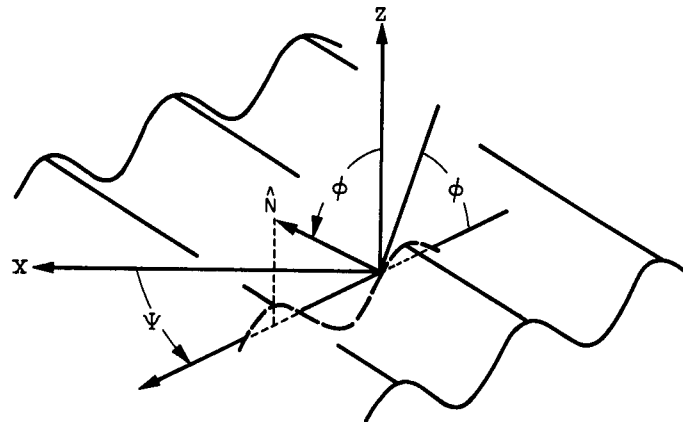


Fig. 2—The local coordinate system for a single sinusoid propagating on the ocean surface in a direction  $\Psi$  with respect to the X axis

XY plane. The normal to the water surface at that point is represented by the unit vector  $\hat{N}$ , making an angle  $\phi$  with respect to the Z axis. In Fig. 2 the angles  $\phi$  are greatly exaggerated. The angles generally encountered in this type of analysis are less than  $15^\circ$ . The maximum rms slope determined in this study was  $14^\circ$ , with an average of  $10^\circ$ . Although steep slopes do exist on the ocean surface, the majority of such slopes are associated with wavelengths shorter than those analyzed here. The steep slopes that do enter into the analysis occur infrequently and degrade the results only slightly. The rationale for this will be explained in the section on Minor Spectral Distortions.

The light that is specularly reflected toward the camera from a facet of water surface comes from a direction represented by the unit vector  $\hat{S}$ . The three vectors  $\hat{C}$ ,  $\hat{N}$ , and  $\hat{S}$  are coplanar, with the angle between  $\hat{C}$  and  $\hat{N}$ , and  $\hat{S}$  and  $\hat{N}$ , being  $\beta$ . The variation of  $\beta$ , and hence of the intensity reflection coefficient of the water surface, with slope angle  $\phi$  is one of the factors enabling the recording of surface slope angles.

Figure 3 shows the variation in the intensity reflection coefficient with  $\beta$  for horizontally polarized light. Thus the light from the sky that is reflected toward the camera is modulated by the slope angle of the water surface. A second factor, which would in theory enable one to record surface slope angles, is the usual, under clear sky or uniformly overcast conditions, monotonic variation of sky brightness with  $\eta$ . The sky is usually brighter at the horizon than at the zenith. Since both the sky brightness and intensity reflection coefficient increase for positive  $\phi$  (away from the camera) and decrease for negative  $\phi$  (toward the camera), the contrast between different slope angles is increased. The presence of broken clouds may degrade the analysis somewhat, that degradation increasing with the brightness fluctuations and the spatial scale of those fluctuations.

The light directed toward the camera from a given point on the surface and from the intervening atmosphere may be expressed by

$$I = b_1 S(\eta, \zeta) R(\beta) + b_2 W(\hat{C}, \phi) + b_3 B, \quad (1)$$

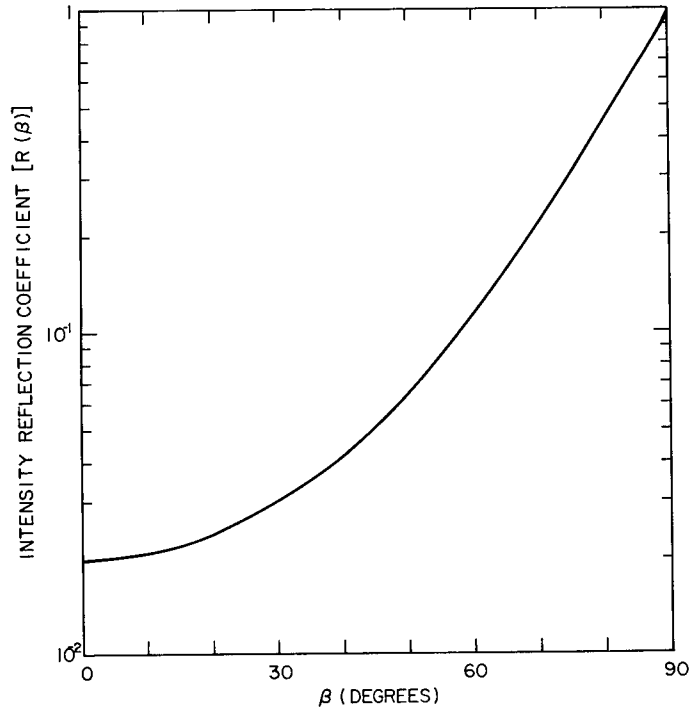


Fig. 3—The variation in the intensity reflection coefficient  $R(\beta)$  with  $\beta$  for horizontally polarized light

where  $I$  is the intensity of the light striking a corresponding point on the film,  $b_1$ ,  $b_2$ , and  $b_3$  are constants that need not be determined in a first-order development for the open ocean,  $S(\eta, \zeta)$  is the brightness of the sky in a direction determined by  $\eta$  and  $\zeta$ ,  $R(\beta)$  is the intensity reflection coefficient for the slope reflecting  $S(\eta, \zeta)$  toward the camera,  $W(\hat{C}, \phi)$  is the intensity of the light scattered upward through the surface making an angle  $\phi$  with the horizontal and in the direction  $\hat{C}$ , and  $B$  is the intensity of light scattered by the intervening atmosphere into the camera. The third term,  $b_3B$ , is relatively uniform over the field of view of the camera, possibly increasing toward the far field. It is however not a function of  $\phi$ . Also, the conditions under which one may obtain good photography are such that the third term is much smaller than the first. Since the third term is not a function of  $\phi$  and its magnitude is very small, its effect on the development that follows will be ignored. The second term is a weak function of  $\phi$  but may have a significant magnitude. Its effect is greatest in turbid waters, where the relative intensity of the light scattered from beneath the water surface and refracted toward the camera is large. Even in this case the variation in  $W(\hat{C}, \phi)$  with  $\phi$  is small compared to the variation of the first term with  $\phi$ . For the nonturbid open ocean the variation of  $W(\hat{C}, \phi)$  with  $\phi$  is very small compared to the variation of the first term with  $\phi$ .

To a first-order approximation the intensity due to a given slope angle is

$$I = I_0 + \left( \frac{\partial I}{\partial \phi} \right)_0 \phi, \quad (2)$$

where the subscript zero indicates that the term is to be evaluated at the analysis angle  $\theta$  with  $\phi = 0$ . A first-order approximation is valid because the slope angles being analyzed are small.

$$\frac{\partial I}{\partial \phi} = b_1 S \frac{\partial R}{\partial \beta} \frac{\partial \beta}{\partial \phi} + b_1 R \frac{\partial S}{\partial \phi} + b_2 \frac{\partial W}{\partial \phi} \quad (3)$$

$$\approx b_1 S \cos \Psi \frac{\partial R}{\partial \beta} + 2b_1 R \cos \Psi \frac{\partial S}{\partial \eta} + b_2 \frac{\partial W}{\partial \phi}, \quad (4)$$

assuming that  $\frac{\partial S}{\partial \xi} \approx 0$ . Hence

$$I = I_0(1 + U_0 \phi \cos \Psi), \quad (5)$$

where the sensitivity function  $U_0$  is

$$U_0 = \left[ b_1 S_0 \left( \frac{\partial R}{\partial \beta} \right)_0 + 2b_1 R_0 \left( \frac{\partial S}{\partial \eta} \right)_0 + \frac{b_2}{\cos \Psi} \left( \frac{\partial W}{\partial \phi} \right)_0 \right] / I_0. \quad (6)$$

The third term in Eq. (6) is very small for the open ocean and may be ignored. The practical value for  $U_0$  is therefore

$$U_0 = \frac{1}{R_0} \left( \frac{\partial R}{\partial \beta} \right)_0 + \frac{2}{S_0} \left( \frac{\partial S}{\partial \eta} \right)_0. \quad (7)$$

This value is nominally 0.1 per degree.

If the sea is photographed on the linear portion of the  $\gamma$  curve ( $D$  vs  $\log E$  curve) of the film, the optical density of the negative is related to  $\phi$  by

$$D = D_0 + \gamma \log (1 + U_0 \phi \cos \Psi). \quad (8)$$

The above development has been carried out for one specific point on the negative. Equation (8) is however an equally good approximation for surrounding points. It may therefore be written

$$D(x, y) = D_0(x, y) + \gamma \log [1 + U_0(x, y) \phi(x, y) \cos \Psi(x, y)] \quad (9)$$

$$= D_0(x, y) + \gamma \log [1 + \phi'(x, y)], \quad (10)$$

where  $x$  and  $y$  are coordinates on the negative and

$$\phi'(x, y) = U_0(x, y) \phi(x, y) \cos \Psi(x, y). \quad (11)$$

## OPTICAL ANALYSIS

The negative that is obtained by photographing the sea is therefore a two-dimensional record of the random surface slopes that are generated by the wind and any swell that may have been present. The most direct method of analyzing such a two-dimensional record is optical analysis.

The system used in this study is outlined in Fig. 4. The He-Ne laser emits red light at a wavelength of 6328 Å. The lens in the spatial filter focuses the beam through a pinhole. The region around the pinhole blocks any nonparallel rays emitted by the laser

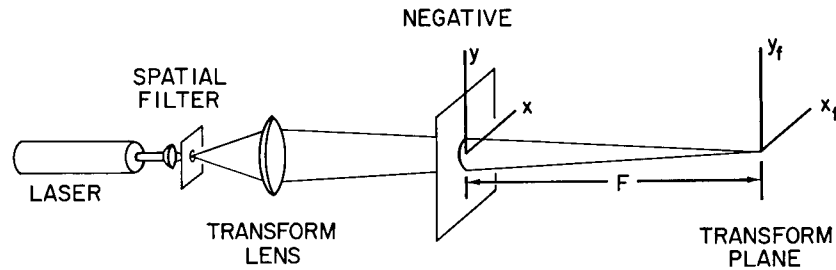


Fig. 4—The system used for optical analysis

which would appear in the transform plane as noise. The transform lens then focuses the light to a point at the transform plane. When a negative is inserted into the converging beam, the density fluctuations representing the random angles of surface slope diffract the light, giving rise to a Fresnel diffraction pattern in a central region about the point imaged by the transform lens. The intensity pattern, a sample of which is shown in Fig. 5, is given analytically by [2]

$$I_f(x_f, y_f) = (\lambda F)^{-2} \left| \int_{-\infty}^{\infty} \int_{-\infty}^{\infty} A(x, y) e^{-j(2\pi/\lambda F)(xx_f + yy_f)} dx dy \right|^2, \quad (12)$$

where  $x_f$  and  $y_f$  are coordinates in the transform plane,  $x$  and  $y$  are coordinates on the negative,  $\lambda$  is the wavelength of the laser light,  $F$  is the distance from the negative to the transform plane, and  $A(x, y)$  is the amplitude of the light immediately after passing through the negative. The pattern, as shown in Fig. 5, is symmetric about the origin, with each of the two lobes containing the same information.

The integral in Eq. (12) is the Fourier transform  $\mathcal{F}$  of  $A(x, y)$ . Hence

$$I_f(x_f, y_f) = (\lambda F)^{-2} \left| \mathcal{F}[A(x, y)] \right|^2. \quad (13)$$

The intensity distribution in the transform plane is then proportional to the Fourier transform squared, or spectrum, of the light amplitude transmitted by the negative. It will be

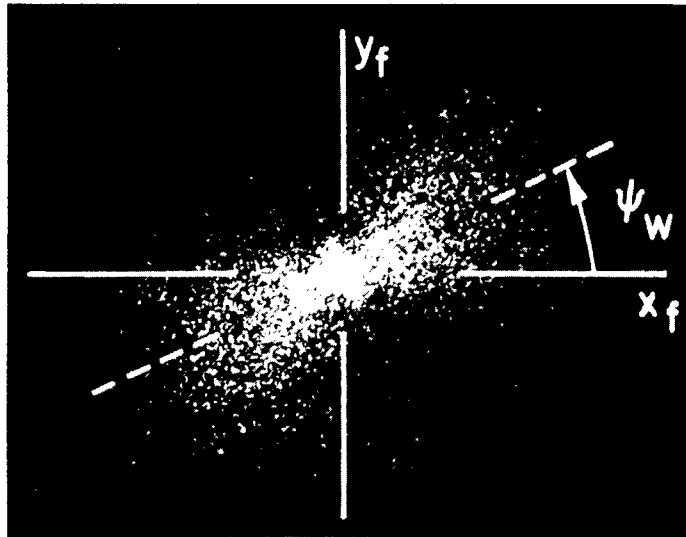


Fig. 5—A representative diffraction pattern-slope spectrum from one negative. The dashed line, oriented at an angle  $\psi_w$  with respect to the  $x_f$  axis, is the average line of symmetry of the intensity distribution.

shown that, in the region of the transform plane to be analyzed, the intensity distribution is proportional to the slope spectrum of the sea.

The amplitude of the light in a laser beam is a gaussian function and may be written

$$A(x, y) = A_0 e^{-(x^2+y^2)/a^2}, \quad (14)$$

where  $A_0$  is the amplitude in the center of the beam,  $x$  and  $y$  are measured perpendicular to, and from the axis of, the beam, and  $a$  is the distance from the axis at which the amplitude is  $1/e$  of that on the axis. Immediately upon passing through the negative the beam has the amplitude

$$A(x, y) = A_0 e^{-(x^2+y^2)/a^2} 10^{-D(x,y)/2} \quad (15)$$

$$= A_0 e^{-(x^2+y^2)/a^2} 10^{-D_0(x,y)/2} [1 + \phi'(x, y)]^{-\gamma/2}. \quad (16)$$

$D_0(x, y)$  is a monotonic function which increases from near to far field. The spatial relationships at the negative are such that the term outside the brackets is a very slightly deformed gaussian beam. Denoting this term by  $g'$ , and in keeping with a first-order development, Eq. (16) becomes

$$A(x, y) = g' - \frac{1}{2}\gamma g' \phi'(x, y). \quad (17)$$

Consequently Eq. (13) may be written

$$I_f(x_f, y_f) = (\lambda F)^{-2} \left\{ |G'|^2 - \gamma \text{Re}[G'(G' \otimes \bar{\phi}')^*] + \frac{1}{4}\gamma^2 |G' \otimes \bar{\phi}'|^2 \right\}, \quad (18)$$

where  $\mathcal{F}(g') = G'$ ,  $\mathcal{F}(\phi') = \bar{\phi}'$ ,  $\text{Re}[\ ]$  indicates the real part of the quantity in brackets, the symbol  $\otimes$  denotes a convolution, and the symbol  $*$  denotes the complex conjugate.

The first term in the braces is centered at the origin and is referred to as the *dc* term. It is the Fourier transform of the distribution of light that impinges on the negative after being slightly deformed by a function of  $D_0(x, y)$ . If the gaussian were not slightly deformed,  $|G'|^2$  would itself be gaussian in shape and, physically, the image of the gaussian distribution of light passing through the pinhole of the spatial filter. The effect of  $D_0(x, y)$  is to very slightly broaden the *dc* term. Nearly all of the light energy transmitted by the negative is focused into this term, giving it a peak intensity 1000 or more times greater than that of the second and third terms combined. It is, however, essentially zero a short distance from the origin. Its effect is inconsequential in the method of analysis used here.

The second term is weighted by  $G'$  and therefore, in the region outside the *dc* term, is small compared to the third term in the square brackets.

The third term gives rise to the bow-tie-shaped pattern shown in Fig. 5. The effect of the convolution is such that each point in the intensity distribution is not a "point" intensity, but rather a "spot" having the same shape as the *dc* term. If the distribution is sampled using a detecting area larger than each convolved spot, Eq. (18) becomes

$$I_f'(x_f, y_f) = (\text{constant}) |\bar{\phi}'|^2, \quad (19)$$

where the prime on  $I_f'$  indicates the distribution outside the *dc* term, when sampled by an appropriately sized detector.

The term  $U_0(x, y)$  in Eq. (11) is very similar in its effects on the diffraction pattern as  $D_0(x, y)$  in Eq. (16).  $U_0(x, y)$  is a monotonically increasing function from near to far range. Writing

$$\bar{\phi}' = \mathcal{F}[U_0(x, y) \phi(x, y) \cos \Psi(x, y)] \quad (20)$$

$$= \mathcal{F}[U_0(x, y)] \otimes \mathcal{F}[\phi(x, y) \cos \Psi(x, y)], \quad (21)$$

it is seen that  $U_0(x, y)$  slightly broadens each convolved spot in the diffraction pattern. Equation (19) then becomes

$$I_f'(x_f, y_f) = (\text{constant}) |\mathcal{F}[\phi(x, y) \cos \Psi(x, y)]|^2 \quad (22)$$

With reference to Fig. 5, the intensity distribution along any radial line at angle  $\psi$  arises from all slope angles having approximately the same  $\Psi$ . Due to perspective the angle  $\psi$  is not equal to  $\Psi$ , but is given by

$$\tan \psi = \frac{\tan \Psi}{\sin \theta} . \quad (23)$$

The dashed line, at an angle  $\psi_w$  with respect to the  $x_f$  axis, is the average line of symmetry of the intensity distribution. If the sea is photographed such that the  $X$  direction is somewhat parallel to the wind direction  $\Psi_w$ , then  $\psi_w$  represents  $\Psi_w$ .

In the type of analysis used in this study the diffraction pattern of each photograph was read along the line defined by  $\psi_w$ . Different points on the negative, however, contribute to the intensity distribution along these lines with slightly different values of  $\Psi(x, y)$ . The effective deviation in  $\Psi(x, y)$  is small, less than  $\pm 2^\circ$ , and  $\cos \Psi(x, y)$  may be considered to be a constant. Equation (22) then becomes

$$I'_f(r, \psi_w) = (\text{constant}) |\mathcal{F}[\phi(x, y)]|^2 , \quad (24)$$

where  $I'_f(r, \psi_w)$  is the intensity along the line defined by  $\psi_w$ , at a distance  $r$  from the origin. The distance  $r$  is inversely proportional to the water wavelengths  $\lambda_w$  on the ocean and may be related to  $k (= 2\pi/\lambda_w)$  when the altitude of the aircraft and certain camera and optical bench parameters are known. Since the surface slope angles being analyzed are small, the angle is essentially equal to the surface slope. The intensity distribution may then be written in a form more familiar to the oceanographer:

$$I'_f(k, \psi_w) = (\text{constant}) \Phi(\phi; k, 0) , \quad (25)$$

where  $\Phi(\phi; k, 0)$  is the slope spectrum of the sea surface, given as a function of  $k$  for slopes in the direction of the wind ( $\Psi - \Psi_w = 0$ ). An example of the distribution  $I'_f$  is shown in Fig. 6.

In the preceding development it has been assumed that the area of the detector sampling the intensity distribution is larger than any convolved "spot." This is not a limitation in the type of analysis used here. Any given negative depicts only a small sample of the random slopes on the ocean surface. The intensity distribution is therefore not uniform, but a pattern of "spots" representing only the wavelengths in the area being analyzed. The detecting area must be large enough to integrate the distribution to yield a reasonably smooth curve, such as shown in Fig. 6.

## THE OCEAN SPECTRUM

The ideal way to analyze the ocean surface, and obtain such parameters as rms wave height and rms slope, would be to obtain one or more negatives depicting an area sufficiently large so that the longest water wavelength present would be shown many times, and at the same time adequately resolve the shortest wavelengths present. Since all slopes present would then be represented many times, a more accurate spectrum could be determined if the negative showed no perspective. Obtaining such a negative is clearly not possible. One could possibly construct the spectrum from a number of negatives,

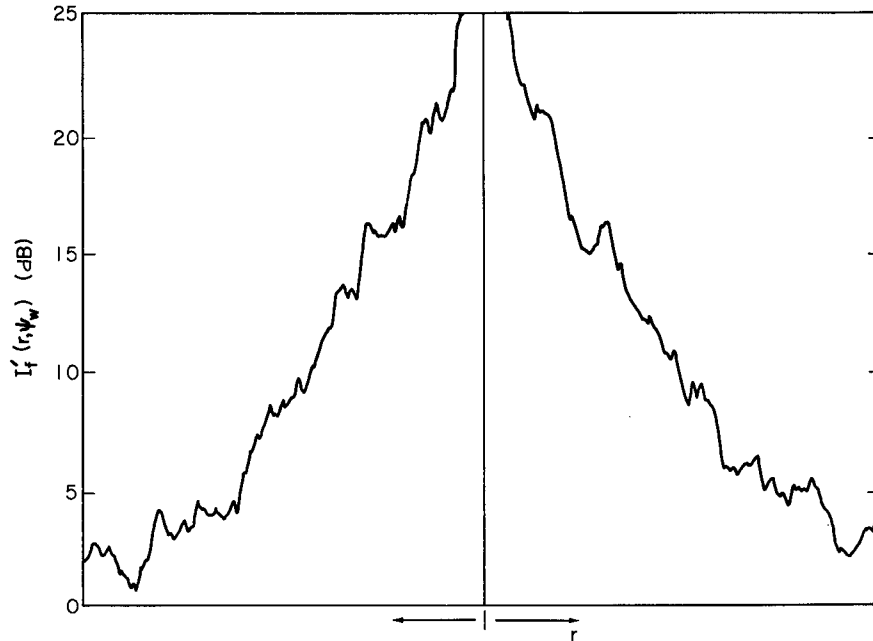


Fig. 6—A representative example of  $I'_f(r, \psi_w)$  vs  $r$

each recording a different wavelength portion of the ocean surface, but such an undertaking would be extremely difficult in practice.

In the type of analyses used here it is necessary to record only one band of wavelengths from roughly 2 to 50 meters. The shape of the optically determined spectrum is then compared to a previously and experimentally determined ocean spectrum in the same wavelength band. Since only the shape of the optical spectrum is used, it is not necessary to determine the constant in Eq. (25). This method effectively extends the limited optical spectrum to all wavelengths, thus yielding a more accurate determination of the ocean surface descriptors.

The ocean spectrum to which the optical spectra were fitted is that determined by W.J. Pierson, Jr., and L. Moskowitz [3]. The wave-height spectrum as a function of frequency is given as

$$\Phi(h; \omega) = 8.1 \times 10^{-3} \left( \frac{g^2}{\omega^5} \right) e^{-\beta g^4 / V^4 \omega^4}, \quad (26)$$

where  $h$  is the wave height (displacement from average surface level),  $\omega$  is the temporal frequency of the wave,  $g$  is the acceleration due to gravity ( $32 \text{ ft s}^{-2}$ ),  $\beta = 0.74$ , and  $V$  is the wind speed measured 64 feet above the mean ocean surface. The spectrum is that for a single point on the ocean surface assuming that the wind has been blowing with an approximately constant speed and direction for a period sufficiently long for the spectrum to be temporally stable.

This spectrum was computed from data assumed to be representative of fully developed seas, generated by winds of 20 to 40 knots. Therefore, the data on which Eq. (26) is based are not representative of the seas analyzed in this program—winds of 3 to 21 knots generating seas that were probably only partially developed. The use of

the spectrum, however, which has not been shown to be invalid at lower wind speeds, yields results consistent with visual observations. For the sea conditions encountered in this program, an experienced observer can estimate the wind speed from whitecap coverage. In all data sets showing whitecapping the wind speed estimated from the appearance of the negatives agreed with that inferred by the type of analysis used here to better than  $\pm 2$  knots. In addition to this type of analysis being more accurate at the lower wind speeds, the correlation between the appearance of the ocean surface and the inferred wind speed is very good. It is therefore considered that the use of the Pierson-Moskowitz spectrum in this program is valid.

The following development will show how a height spectrum may be transformed into a slope spectrum. As a definition, consider any quantity of the form  $\Phi(a; b, c)$  to be the spectrum of the measurable  $a$  as a function of  $b$  and  $c$ . Since both a one-dimensional height spectrum (as in Eq. (26)) and a two-dimensional height spectrum (two-dimensional as in the case of an optical spectrum) of the same surface must yield the same rms wave height  $\sigma_h$ ,

$$\sigma_h^2 \equiv \int_0^{\infty} \Phi(h; \omega) d\omega \quad (27)$$

$$\equiv \int_0^{\infty} \int_0^{2\pi} \Phi(h; k, \alpha) k dk d\alpha \quad (28)$$

$$= \int_0^{\infty} A(k, \alpha) k dk , \quad (29)$$

where

$$A(k, \alpha) = \int_0^{2\pi} \Phi(h; k, \alpha) d\alpha \quad \left( k = \frac{2\pi}{\lambda} \right) \quad (30)$$

and

$$\alpha = \Psi - \Psi_w . \quad (31)$$

Therefore

$$\Phi(h; \omega) d\omega = A(k, \alpha) k dk . \quad (32)$$

For the wavelengths being analyzed  $\omega^2 = gk$ . Hence

$$\Phi(h; \omega) = \left( \frac{2\omega^3}{g^2} \right) \int_0^{2\pi} \Phi(h; k, \alpha) d\alpha . \quad (33)$$

Since

$$\Phi(h; k, \alpha) = k^{-2} \Phi(\phi; k, \alpha) , \quad (34)$$

Eq. (33) becomes

$$\Phi(h; \omega) = \left(\frac{2}{\omega}\right) \int_0^{2\pi} \Phi(\phi; k, \alpha) d\alpha . \quad (35)$$

At the wavelengths being analyzed the slope spectrum may be factored:

$$\Phi(\phi; k, \alpha) = \Phi(\phi; k, 0) \times \mathcal{L}(\alpha) , \quad (36)$$

where

$$\int_0^{2\pi} \mathcal{L}(\alpha) d\alpha = C_1 = \text{constant} . \quad (37)$$

Therefore

$$\Phi(h; \omega) = \left(\frac{2C_1}{\omega}\right) \Phi(\phi; k, 0). \quad (38)$$

Using Eq. (26) and  $\omega^2 = gk$ ,

$$\Phi(\phi; k, 0) = \left(\frac{4.05 \times 10^{-3}}{C_1}\right) \left(\frac{g^2}{\omega^4}\right) e^{-\beta g^4/V^4 \omega^4} \quad (39)$$

$$= (\text{constant}) k^{-2} e^{-\beta g^2/V^4 k^2} . \quad (40)$$

Therefore, from Eq. (25), the intensity distribution along the line of symmetry in the optical diffraction pattern should be of the form

$$I'_f(k, \psi_w) = (\text{constant}) k^{-2} e^{-\beta g^2/V^4 k^2} \quad (41)$$

for the range of water wavelengths adequately recorded.

The Neumann form for the wave-height spectrum was used prior to the adoption of the Pierson-Moskowitz spectrum. It was used to analyze the photography of 1 May 1971. It has subsequently been shown that the surface descriptors derived from both forms agree very well. The Neumann form is [4]

$$\Phi(h; \omega) = \left(\frac{C\pi}{2}\right) \omega^{-6} e^{-2g^2/V^2 \omega^2} , \quad (42)$$

where  $C \approx 32.8 \text{ ft}^2 \text{ s}^{-5}$ . From Eq. (42), (38), and (25),

$$I'_f(k, \psi_w) = (\text{constant}) k^{-1/2} e^{-2g/Vk^2} . \quad (43)$$

Knowing the form that  $I'_f(k, \psi_w)$  should have, the wind speed  $V$  may be determined by fitting the two curves, using either Eq. (41) or Eq. (43). The following discussion will consider only the Pierson-Moskowitz form, Eq. (41). Equation (41) may be rewritten as

$$k^2 I'_f(k, \psi_w) \propto e^{-\beta g^2 / V^4 k^2} \quad (44)$$

where the symbol "α" means "varies as." This is the form actually used in fitting the two curves to determine  $V$ . The exponential rises sharply as a function of  $k$  and then bends to a slowly increasing function for large  $k$ . The bend, or knee, of the curve is used to fit the two sides of Eq. (44).

The data used by Pierson and Moskowitz to obtain the wave-height spectrum were analyzed separately by Moskowitz [5] to yield the significant wave height as a function of wind speed. The functional relationships between the significant wave height, the rms wave height  $\sigma_h$ , and the wind speed  $V$  (Eq. (1) and (10) of Ref. 5) are such that

$$\sigma_h = 0.00455 V^2$$

in units of feet if  $V$  is given in knots.

The rms slope of the ocean surface is also a function of wind speed. The rms slope in the upwind direction, the rms slope in the crosswind direction, and the total rms slope have been determined empirically by Cox and Munk [6] to be

$$\text{rms slope (upwind)} = 0.1 \sqrt{0.163 V}, \quad (46)$$

$$\text{rms slope (crosswind)} = 0.1 \sqrt{0.3 + 0.099 V}, \quad (47)$$

$$\text{rms slope (total)} = 0.1 \sqrt{0.3 + 0.264 V} \quad (48)$$

in units of radians if  $V$  is given in knots. The wind speeds used to develop the preceding equations were measured at 42 feet above the surface. The difference in wind speed however between 64 feet and 42 feet above the surface is small. In addition, the rms slope is a weak function of wind speed. The use of the wind speed inferred from Eq. (25) introduces a very slight error that is within the experimental error of this type of analysis.

The Boeing Company, which is using the ground truth surface descriptors supplied by NRL to correlate electromagnetic scattering with predictions based on the Kirchhoff approximation, has requested that rms slopes for "slick surfaces" be included in this report. The Kirchhoff approximation assumes the radius of curvature of the scattering facets, and hence the water wavelengths considered, to be much larger than the electromagnetic wavelength. The electromagnetic wavelength at  $L$  band is about 8 inches; thus it may be necessary to consider only the rms slope due to longer wavelengths. Rms slope equations resulting from data taken over oil slicks have also been given by Cox and Munk [6]. The oil slicks effectively eliminated wavelengths shorter than 1 foot, yielding

$$\text{rms slope (upwind)} = 0.1 \sqrt{0.5 + 0.040 V}, \quad (49)$$

$$\text{rms slope (crosswind)} = 0.1 \sqrt{0.3 + 0.043 V}, \quad (50)$$

$$\text{rms slope (total)} = 0.1 \sqrt{0.8 + 0.080 V} \quad (51)$$

in units of radians if  $V$  is given in knots. The values reported here have been calculated from Eq. (48) and (51).

Recent radar data and a few spectral forms suggest values for the rms slope 50% greater than those given by Eq. (48). However Eq. (48) and those indicating higher rms slopes have been used successfully both experimentally and in various theoretical models. It is therefore expected that the true rms slope for a clean surface would be in the range from those figures given in this report to values 50% higher. It is not known whether a like adjustment in Eq. (49) through (51) would be valid.

The total rms slope associated with a given band of water wavelengths  $\lambda_1$  to  $\lambda_2$  may also be calculated from the equation

$$[\text{rms slope } (\lambda_1, \lambda_2)]^2 = 9.27 \times 10^{-4} V \int_{x_1}^{x_2} x^{-1/2} e^{-x} dx, \quad (52)$$

where the rms slope is in radians if  $V$  is given in knots and where

$$x_1 = 3.60 \frac{\lambda_1}{V^2} \quad (53)$$

and

$$x_2 = 3.60 \frac{\lambda_2}{V^2}, \quad (54)$$

in which  $\lambda$  is given in feet. Equation (49) may be derived by multiplying Eq. (42) by  $k^2$  and integrating from  $\omega_1$  to  $\omega_2$  using  $\omega^2 = gk$ ,  $x = 2g^2/V^2\omega^2$ , and  $k = 2\pi/\lambda$ . This equation is not valid for narrow wavelength bands below 1 or 2 feet. When  $\lambda_1 = 0$  and  $\lambda_2 = \infty$ , Eq. (52) yields a total rms slope

$$\text{rms slope (total)} = 0.1 \sqrt{0.164 V}. \quad (55)$$

This value is low compared to that given by Cox and Munk, which itself may be low. Any value calculated using Eq. (52) should therefore be increased by an appropriate, wind-speed and bandwidth dependent, factor. This factor is unknown at present. Its value may be approximated by comparing various figures given by Eq. (52) to the values given by Cox and Munk.

The wave-height spectrum depends on the wind speed at 64 feet and may be given as a function of wave number. The functional relationship is

$$\Phi(h; k) = 0.0041 k^{-3} e^{95/V^4 k^2}, \quad (56)$$

which has the units of feet cubed when  $k$  is given in inverse feet and  $V$  is given in knots.

## COMPUTER ANALYSIS

There are three circumstances in which the optical diffraction pattern cannot be properly analyzed. The first of these circumstances occurs when the knee of the curve, Eq. (44), is at the long water wavelengths and is hidden within the  $dc$  term. The intensity distribution beyond the knee cannot be fitted to the known spectrum with any degree of

validity. The second circumstance arises when the diffraction pattern is weak and most of the distribution is at intensities below the noise level of the detector. In such cases the distribution cannot be adequately defined. The third circumstance occurs when whitecaps are present. They appear on the film as randomly shaped and spaced black patches having a very high contrast with respect to the waves. The whitecaps therefore produce a random diffraction pattern which, due to the higher contrast, is sufficiently high in intensity to partially mask that due to the surface slope angles. The diffraction pattern due to the whitecaps cannot be included in the analysis because the form of the slope spectrum to which the patterns are fitted was derived from a wave-height spectrum. It does not include the random and wildly fluctuating slopes present in a whitecap. If one attempts to optically analyze an area of the surface showing no whitecapping, one must exclude the slightly rougher areas of the ocean surface in the vicinity of the whitecaps that are included in the derived slope spectrum. The surface descriptors so determined would be those of a much calmer sea.

Those sets of photography falling into one or more of the above categories were analyzed by computer. Each set was inspected visually and/or qualitatively by optical analysis to determine the direction of the wind. A microdensitometer was then used to obtain a trace of optical density versus distance on the film from near to far range. A single trace in the direction of the wind was obtained for each negative. The aperture at the negative was a slit 0.05 mm wide in the direction of the trace and 0.60 mm long. The slit was long enough to integrate out the slopes in directions other than the direction of the wind and narrow enough to reproduce the desired slopes with adequate fidelity. Individual whitecaps could then be removed by drawing dummy slope profiles under each whitecap. The profiles on each side of the whitecap would remain to contribute to the spectrum. The traces were then digitized. Each trace covered approximately 2/3 the length of the negative. This was done to adequately sample the long wavelengths.

Since the length of the trace, approximately 25 mm, was more than double the linear dimension of the area used in optical analysis, nominally 11 mm, three steps had to be taken to reduce distortions in the subsequently computed spectrum. The overall slope of the trace,  $D_0(x, y)$  in Eq. (10), and the average value were removed. These two steps greatly reduce the spectral "noise" at low frequencies and produce the equivalent of a much tighter  $dc$  term in optical analysis. Perspective, which shortens wavelengths at far range compared to those at near range, was also removed. This is necessary when analyzing a long trace to prevent overintegration in the spectrum.

The density differences embodied in the final traces were small; consequently the traces were equivalent to those of  $\phi(x, y)$  versus distance on the mean ocean surface. Each trace was then analyzed by means of a Fast Fourier Transform program to yield a curve equivalent to the intensity distribution arrived at in optical analysis, Eq. (24). Since the individual transforms were representative of only single traces through a given negative, the curves fluctuated wildly as a function of  $k(= 2\pi/\lambda)$  and could not be fitted reliably to a known spectrum. Consequently all of the spectra obtained for a given set of photographs had to be averaged to yield a single spectrum. This spectrum was then fitted to the known spectrum to determine the required surface descriptors.

#### MINOR SPECTRAL DISTORTIONS

Several minor distortions in the experimental spectrum and ways to avoid their effects will now be discussed. Most of these arise from the manner in which the sea is

photographed. They will be discussed from the viewpoint of optical analysis, the effect on the computer analysis being equivalent.

The overall density gradient on the negative,  $D_0(x, y)$  in Eq. (10), and the variation of the sensitivity function,  $U_0(x, y)$  in Eq. (11), have been discussed in the section on Optical Analysis and have been shown to place an inconsequential limit on one's ability to measure the intensity distribution close to the origin of the diffraction pattern and to place a lower limit, which is also inconsequential in practice, on the area of the detector used to sample the diffraction pattern. Neither of these two functions actually distort the smoothed spectrum required here.

The distance from the origin in the optical diffraction pattern is proportional to the spatial frequency of the waves as recorded on the negative. Thus the region near the origin corresponds to the low-frequency, or long, water wavelengths; and as one passes outward from the origin, the points correspond to higher frequency, shorter, waves. The perspective with which the ocean surface is recorded on the negative thus introduces a distortion into the spectrum. If the same wavelength were present everywhere on the surface depicted by the negative, the waves at far range would appear closer together and would diffract the light farther from the origin than would the same waves at nearer ranges. Therefore the "spot" in the transform plane corresponding to a given wavelength is "smeared" in the direction from near to far range. It therefore introduces a slight integrating factor into the spectrum. However, it is usually necessary to integrate the spectrum to an even greater degree, through the use of a larger detecting area, to obtain a reasonably smooth curve to fit to the known spectral form.

Since the water waves have a finite height and are photographed obliquely, the waveform is slightly distorted to favor slopes directed toward the camera. The distortion however is small, and the intensity added to the high frequency portion of the spectrum by this distortion is minimal.

The steeper than normal slopes that are associated with the shorter wavelengths could diffract a considerable amount of light energy into the high-frequency portion of the diffraction pattern. This of course depends on whether the short wavelengths are resolved on the negative. If these short waves are present but not resolved, they may also add to the intensity in the high-frequency portion by distorting the recorded slope angles. A facet of the surface covered by unresolved waves is recorded at a density indicative of a facet sloped slightly more toward the camera. The steep slopes that infrequently occur on the longer wavelengths, and are not adequately represented by the first-order theory, also increase the intensity in the high-frequency portion of the diffraction pattern. Film grain too increases the intensity in the high-frequency portion of the diffraction pattern. Film grain has essentially the same effect as a large number of nearly uniformly dispersed, extremely small whitecaps. The diffraction pattern of the film grain is random, but since the grains are of necessity smaller than the finest detail to be analyzed, it contributes to the spectrum only at very high spatial frequencies. The presence of haze in the atmosphere when the photographs are taken has the opposite effect on the high-frequency portion of the diffraction pattern. It reduces the resolution on the negative and smooths the angularity of the randomly deformed water surface. The intensity in the high-frequency portion is thus reduced by the presence of haze.

The five effects mentioned in the preceding paragraph make the high-frequency portion of the experimental spectrum somewhat ambiguous. This can be avoided by placing the emphasis of the analysis on the low-frequency portion. Since the knee of the

curve, Eq. (44), falls within the low-frequency portion of the spectrum in the vast majority of cases, the ambiguity is of little consequence in this type of analysis.

## DATA ANALYSIS

An inventory of test film and photographs taken by FAA and submitted for analysis is given in Table 1. The first nine rolls of film were obtained in testing the camera system to be used and in gaining experience in the techniques of photography necessary for Sea Photo Analysis. Twenty sets of data film and three rolls of test film were submitted after the preliminary test period. Four of the data sets were not suitable for analysis, as explained below. A representative aerial photograph from each of the sixteen data sets analyzed is shown in Figs. 7a through 7p. The photographs were taken from an altitude of 1000 feet, showing an area roughly 600 feet by 1600 feet at a mean depression angle of  $35^\circ$  ( $40^\circ$  in Figs. 7m through 7p).

Table 1  
Inventory of Data Film

Date	Roll	Comments*
4-9-71	1	Resolution test
	2	Overexposed, sun glitter
	3	Overexposed, sun glitter
	4	Overexposed
	5	Overexposed, camera tests
4-16-71	6	Camera tests
	7	Overexposed, sun glitter
4-30-71	-	Camera tests
5-1-71	1	Test film
	2	Group 4 analyzed optically
5-24-71	1, 2	Group 7 analyzed by computer
5-25-71	2, 3	Group 4 analyzed by computer
5-26-71	4, 5	Group 5 analyzed by computer
7-12-71	-	Camera tests
7-26-71	-	Camera tests
9-1-71	1	Degraded imagery
9-2-71	2	Group 3 analyzed optically
9-3-71	3	Degraded imagery
9-22-71	-	Group 6 analyzed optically
10-13-71	1	Group 3 analyzed optically
10-14-71	2	Group 3 analyzed optically
10-15-71	3	Group 3 analyzed optically
3-4-72	1	Group 6 analyzed by computer
3-7-72	2	Group 5 analyzed by computer
3-8-72	3	Group 6 analyzed optically
4-20-72	1, 2	Group 2 analyzed by computer
4-21-72	3, 4	Group 2 analyzed optically
4-22-72	5, 6	Group 1 analyzed by computer
4-24-72	7, 8	Group 1 analyzed optically
4-24-72	9	Camera calibration
5-17-72	1	Wrong polarization
5-18-72	2	Wrong polarization

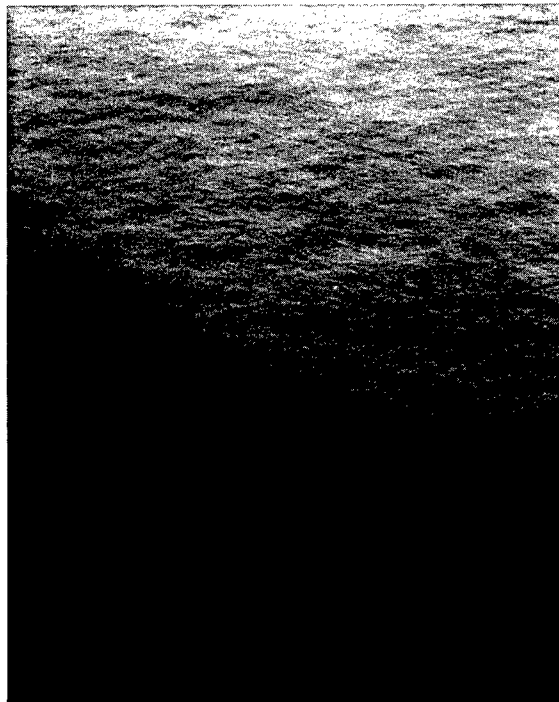
\*The comments are explained in the test.



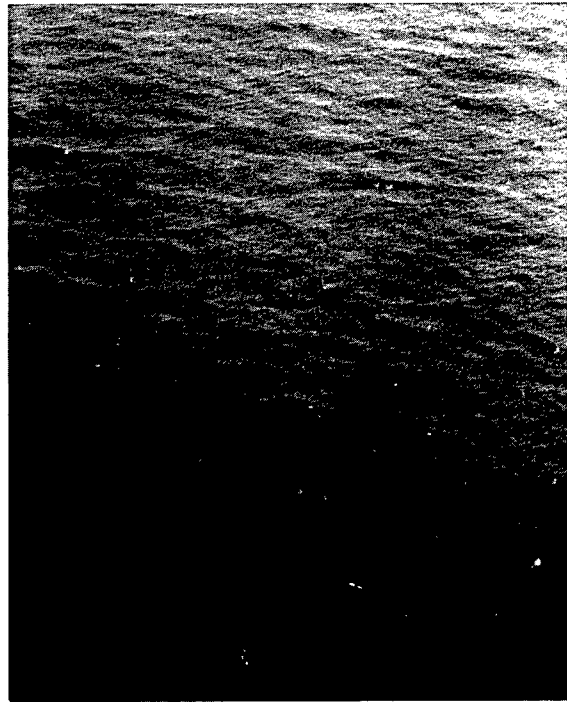
(a) 1 May 1971



(b) 24 May 1971

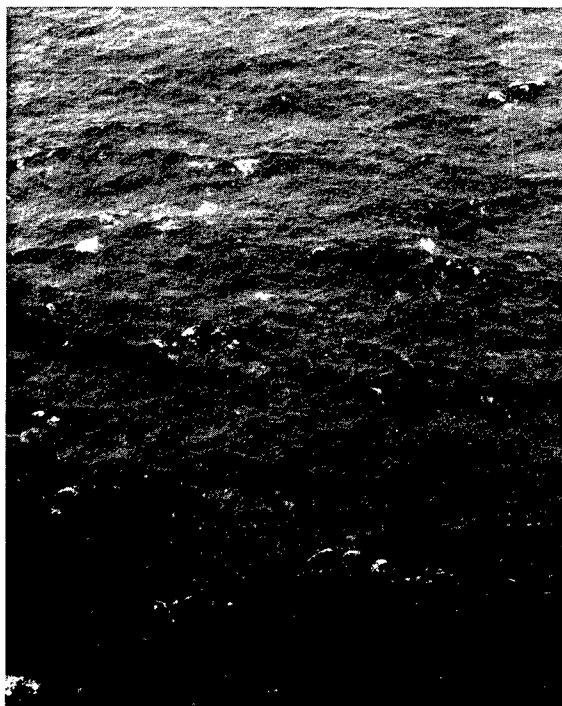


(c) 25 May 1971

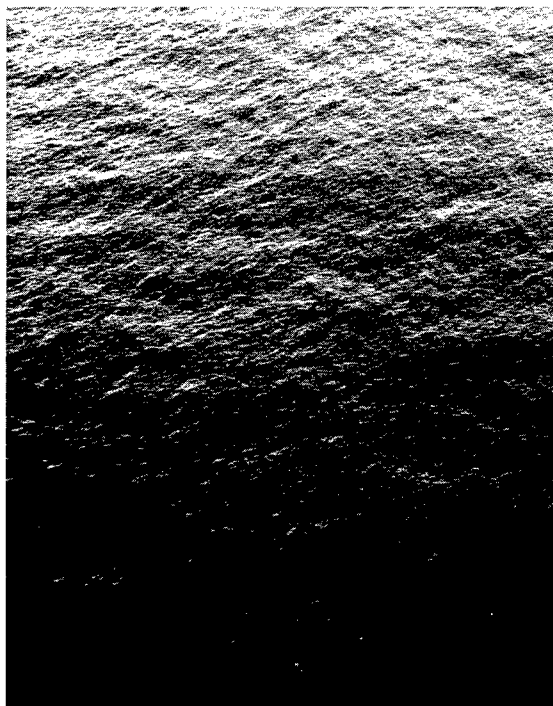


(d) 26 May 1971

Fig. 7—Representative aerial photography from each of the data sets analyzed.  
(Figure continues.)



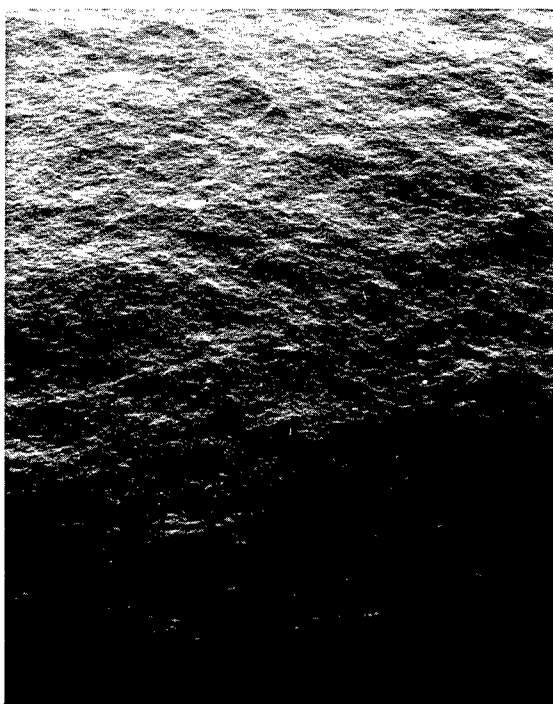
(e) 2 September 1971



(f) 22 September 1971

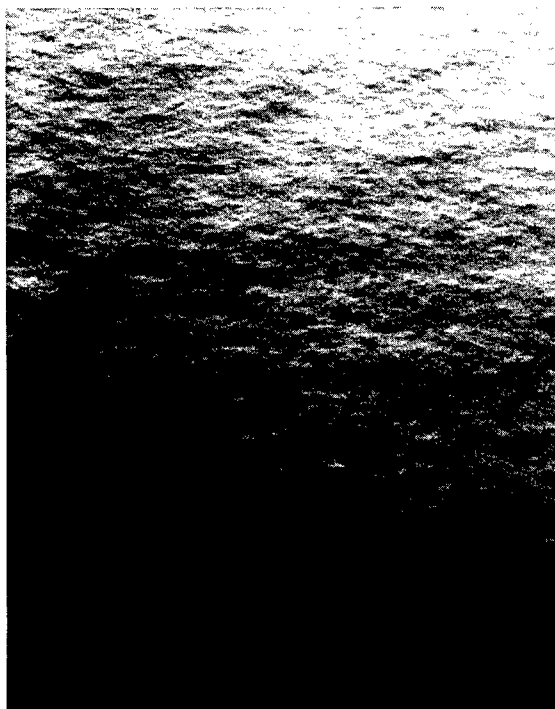


(g) 13 October 1971



(h) 14 October 1971

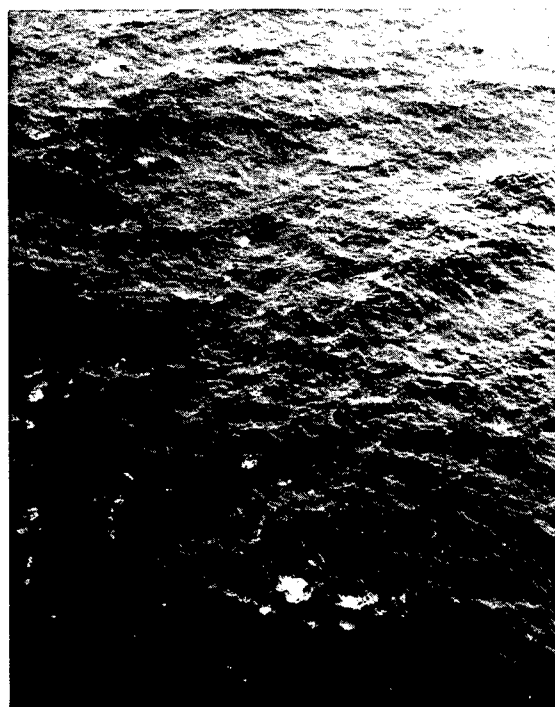
Fig. 7 (Continued)—Representative aerial photography from each of the data sets analyzed.  
(Figure continues.)



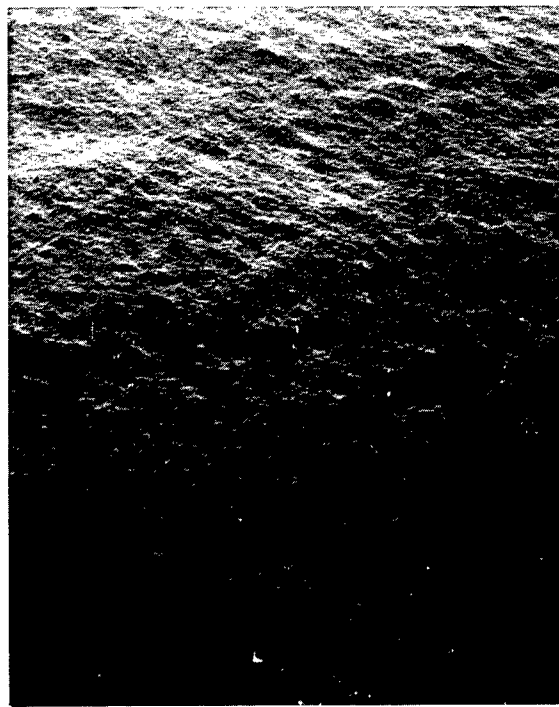
(i) 15 October 1971



(j) 4 March 1972

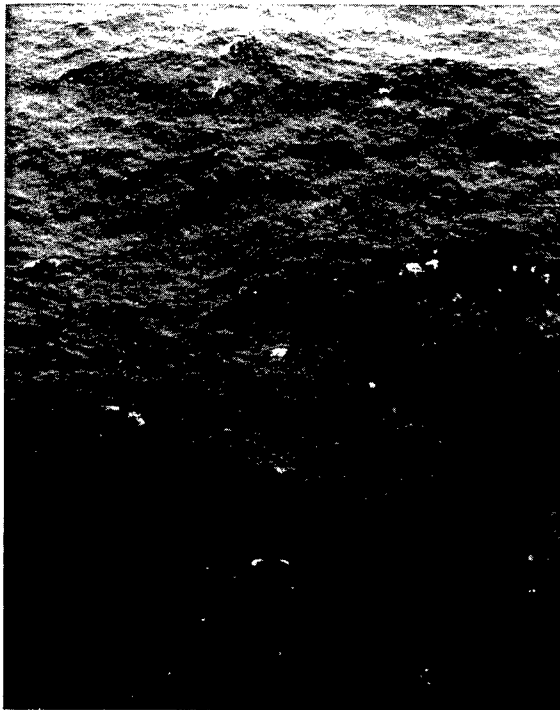


(k) 7 March 1972

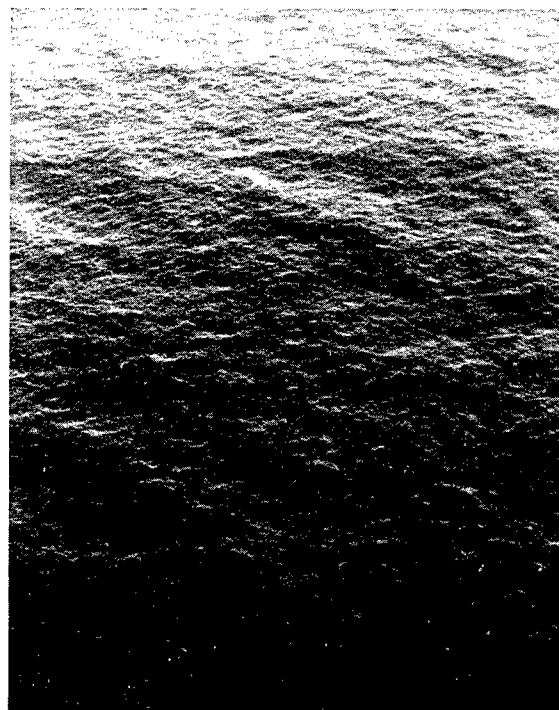


(l) 8 March 1972

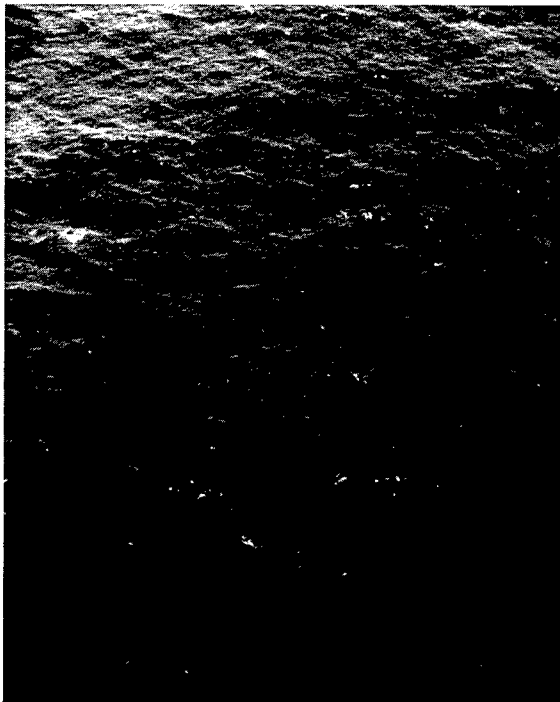
Fig. 7 (Continued)—Representative aerial photographs for each of the data sets analyzed.  
(Figure continues.)



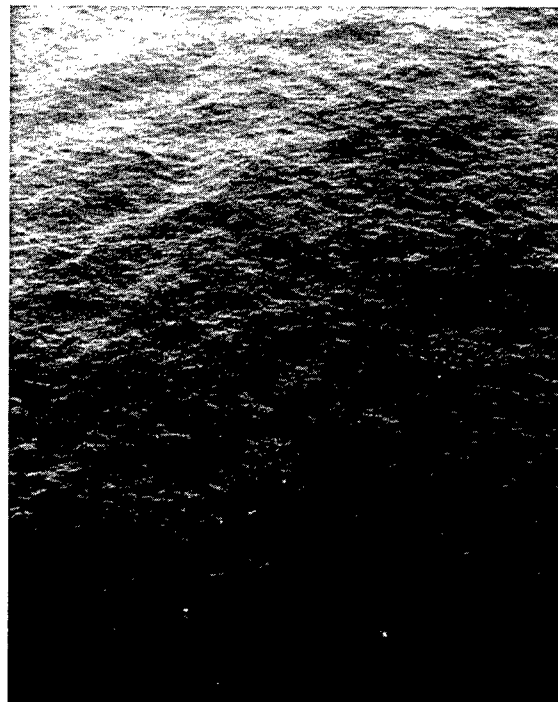
(m) 20 April 1972



(n) 21 April 1972



(o) 22 April 1972



(p) 24 April 1972

Fig. 7 (Concluded)—Representative aerial photographs from each of the data sets analyzed.

As noted in Table 1, the photographs in three of the preliminary data sets showed sun glitter patterns. Sun glitter is the specular reflection of the sun directly toward the camera. On the negative it appears as black spots distributed randomly around a central point. In general the spots decrease in size and are spaced farther apart with increasing distance from the central point. Since the distribution is random from frame to frame, the diffraction patterns are likewise random. Also, since the contrast between the very black spots and the much lighter surrounding image of the waves is much greater than that due to wave slopes, the intensity of the extraneous diffraction pattern due to the glitter partially masks that due to the waves. These two factors would make it very difficult to extract the desired spectrum. In addition, those slopes reflecting sunlight directly toward the camera are effectively removed from the slope analysis, thus distorting the spectrum somewhat. For these reasons it is necessary to obtain photographs of the ocean surface that do not show glitter patterns. This still leaves approximately  $270^\circ$  of the  $360^\circ$  of azimuthal directions available for photography.

The photographs obtained on 1 and 3 September 1971 were degraded by condensation and hydraulic oil on the window through which the ocean surface was photographed. Foreign fluids on the window effectively smear the images of the shorter wavelengths, removing them from the analysis, and could introduce density variations on the film that would distort the long wavelength analysis. Thus such data sets are not suitable for analysis.

The photographs of 17 and 18 May 1972 were obtained with the polarizer placed over the camera lens in the wrong orientation. The surface was therefore photographed using vertically polarized light instead of horizontally polarized light. The intensity reflection coefficient curve corresponding to Fig. 3 for horizontally polarized light would have the same values at  $0^\circ$  and  $90^\circ$ , but would go to zero at Brewster's angle,  $53^\circ$ . Therefore  $R(\beta)$ , maintaining a mean depression angle of  $40^\circ$ , would be double valued. In addition the mean light level and both the magnitude and directionality of the wave-slope sensitivity would change as a function of position on the film. The theory required to analyze such data sets has not been developed.

Eight of the data sets were analyzed optically, as noted in Table 1. The photographs obtained on 1 May, 22 September, and 13, 14, and 15 October 1971 contained an insufficient number of analyzable frames to warrant temporal plots of the ocean descriptors. The minimum, average and maximum values of the descriptors obtained from the few usable frames are given in Table 2. The five sets of descriptors inferred from the 1 May 1971 photography is given in Table 3.

The surface descriptors inferred from the three remaining data sets that could be analyzed optically, 8 March 1972 and 21 and 24 April 1972, are given in Table 2 and are plotted as a function of time and distance in Figs. 8 through 16. Error bars are shown in Figs. 8 and 9. They represent the expected error associated with only one step in the analysis procedure, namely that of fitting the intensity distribution of the diffraction pattern to the accepted spectral form, and are indicative of the corresponding expected error in the other sets reported here. They are shown as an indication of the agreement between the ocean surface to be described and the spectral form used to obtain rms wave height and rms slope.

Table 2  
Inferred Ocean Surface Descriptors

Date	Time (GMT)	Averaged Heading of Waves (deg)	Wind Speed at 64 ft* (knots)	RMS Wave Height* (ft)	RMS Slope* (radians)	
					Clean Surface	Slick Surface†
5-1-71	1812	020	3.3	0.050	0.11	0.10
			3.9	0.069	0.12	0.11
			4.3	0.084	0.12	0.11
5-24-71	1858	132	21.4	2.1	0.24	0.16
5-25-71	2056	086	6.4	0.19	0.14	0.11
5-26-71	1632	020	12.4	0.70	0.19	0.13
9-2-71	1921	090	14.7	0.98	0.20	0.14
9-22-71	1720	267	6.4	0.19	0.14	0.11
			7.0	0.22	0.15	0.12
			7.5	0.26	0.15	0.12
10-13-71	1821	180	8.0	0.29	0.16	0.12
			10.7	0.52	0.18	0.13
			14.9	1.0	0.21	0.14
10-14-71	1827	135	9.2	0.39	0.17	0.12
			10.1	0.46	0.17	0.13
			11.2	0.57	0.18	0.13
10-15-71	1924	040	8.4	0.32	0.16	0.12
			10.0	0.46	0.17	0.13
			11.6	0.61	0.18	0.13
3-4-72	1703	160	18.2	1.5	0.23	0.15
3-7-72	1620	147	14.5	0.96	0.20	0.14
3-8-72	1853	030	6.1	0.17	0.14	0.11
			6.9	0.22	0.16	0.12
			8.5	0.33	0.16	0.12
4-20-72	1812	123	14.3	0.93	0.20	0.14
4-21-72	1721	100	6.6	0.20	0.14	0.12
			6.9	0.22	0.15	0.12
			7.1	0.23	0.15	0.12
4-22-72	1732	113	14.9	1.0	0.21	0.14
4-24-72	1709	110	5.2	0.12	0.13	0.11
			5.7	0.15	0.13	0.11
			6.1	0.17	0.14	0.11

\*When three values are given for any one quantity they represent the minimum, average, and maximum values for the data set.

†Rms slope due to wavelengths longer than 1 foot.

Computer analysis was required on the eight remaining data sets, 24, 25, and 26 May 1971, 2 September 1971, 4 and 7 March 1972, and 20 and 22 April 1972. Consequently, only the average values for wind speed, rms wave height, and rms slope (clean and slick surface) are given in Table 2.

Table 3  
Comparison of Descriptors Inferred From the Pierson-Moskowitz Spectrum  
and From the Neumann Spectrum\*

Time (GMT)	Windspeed at 64 ft (knots)		RMS Wave Height (ft)		RMS Slope (radians)			
	Pierson- Moskowitz	Neumann	Pierson- Moskowitz	Neumann	Clean Surface		Slick Surface	
					Pierson- Moskowitz	Neumann	Pierson- Moskowitz	Neumann
18:11:59	4.0	4.3	0.073	0.084	0.12	0.12	0.11	0.11
18:12:01	3.8	4.0	0.066	0.073	0.11	0.12	0.11	0.11
18:12:03	4.3	4.5	0.084	0.092	0.12	0.12	0.11	0.11
18:12:05	4.0	4.3	0.073	0.084	0.12	0.12	0.11	0.11
18:12:07	4.0	4.3	0.073	0.084	0.12	0.12	0.11	0.11
18:13:04	3.3	3.3	0.050	0.050	0.11	0.11	0.10	0.10

\*Obtained from the 1 May 1971 Photographs (Roll 2, Group 4). The Averaged Heading of the Waves was 20°.

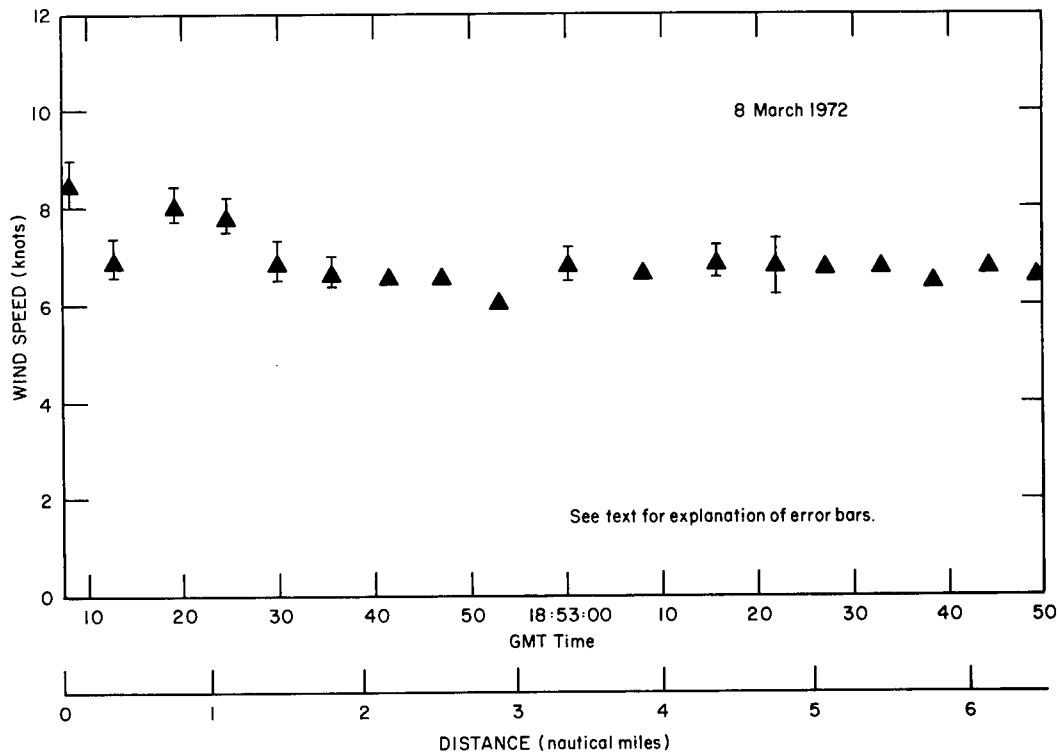


Fig. 8—The inferred wind speed as a function of time and distance for 8 March 1972

The wind speeds inferred from Eq. (44) appear to be quite accurate, based on the fact that an experienced observer can estimate the wind speed quite well when whitecaps are present. In all data sets showing whitecapping the estimate agreed with that derived from Eq. (44) to better than  $\pm 2$  knots. In addition to this type of analysis being more accurate at the lower windspeeds, the correlation between the appearance of the ocean surface and the inferred wind speed is very good. The values computed for the rms wave height and rms

slope should therefore be reliable (keeping in mind that the rms slope given by Cox and Munk may be low). The last figure given for each value is in doubt.

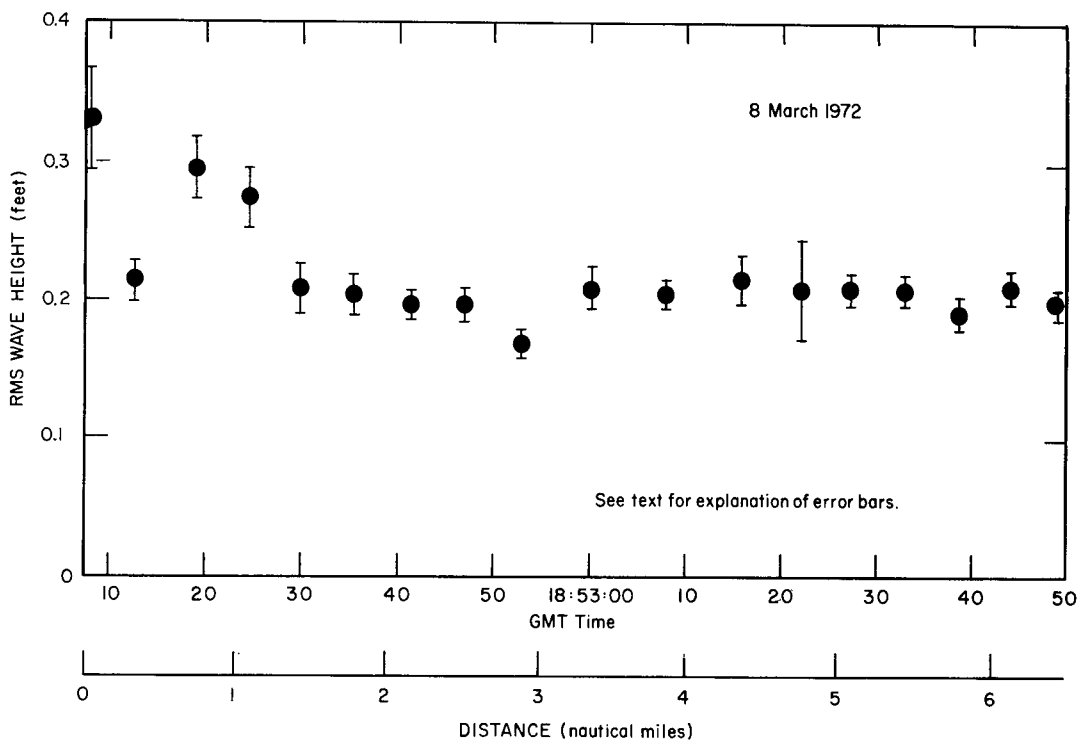


Fig. 9—The inferred rms wave height as a function of time and distance for 8 March 1972

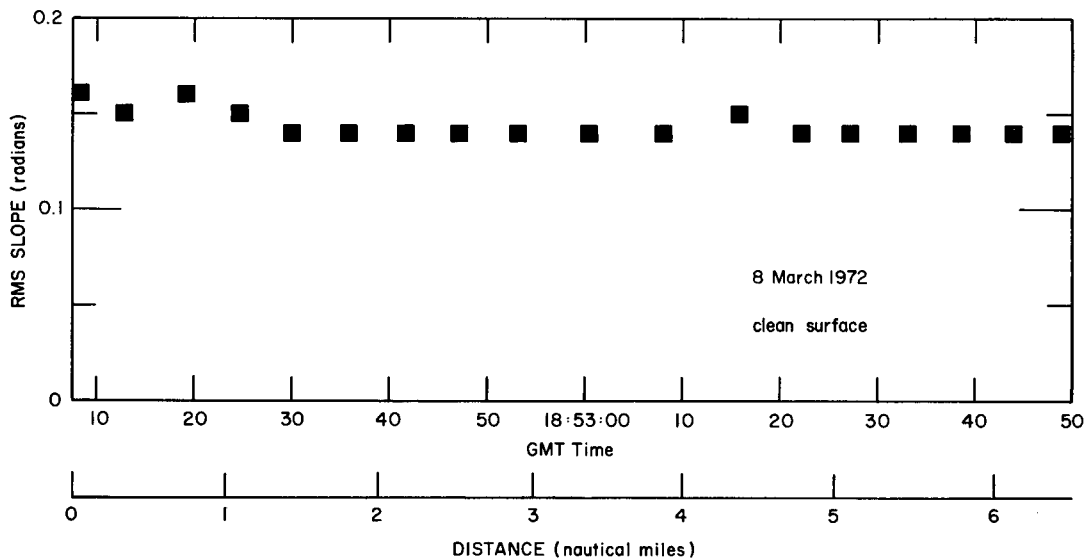


Fig. 10—The inferred rms slope as a function of time and distance for 8 March 1972

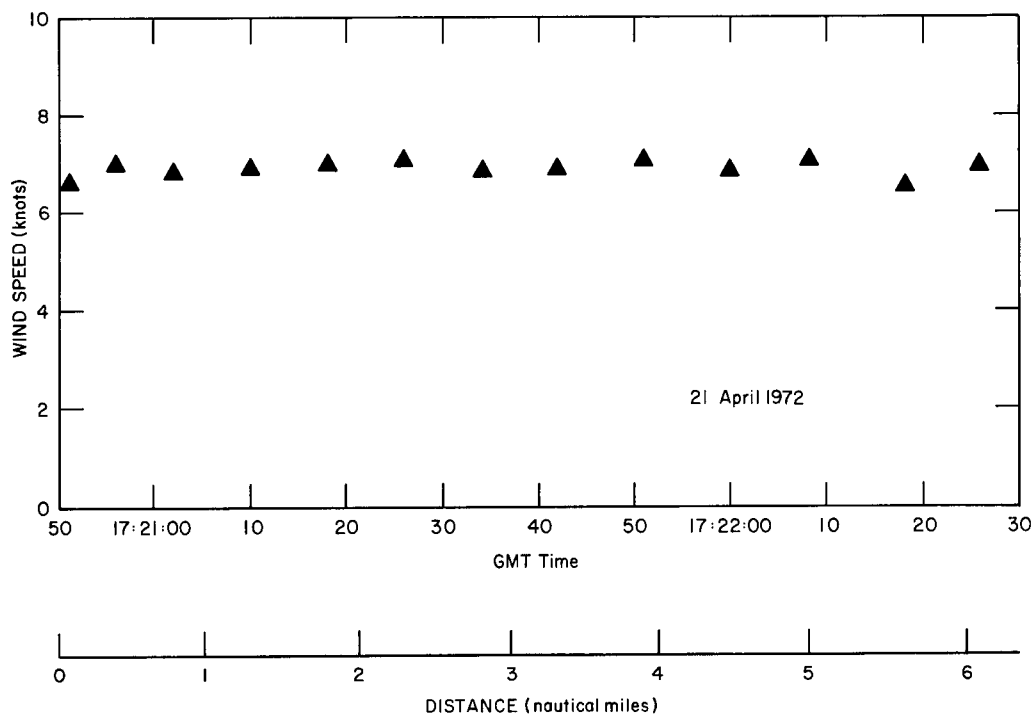


Fig. 11—The inferred wind speed as a function of time and distance for 21 April 1972

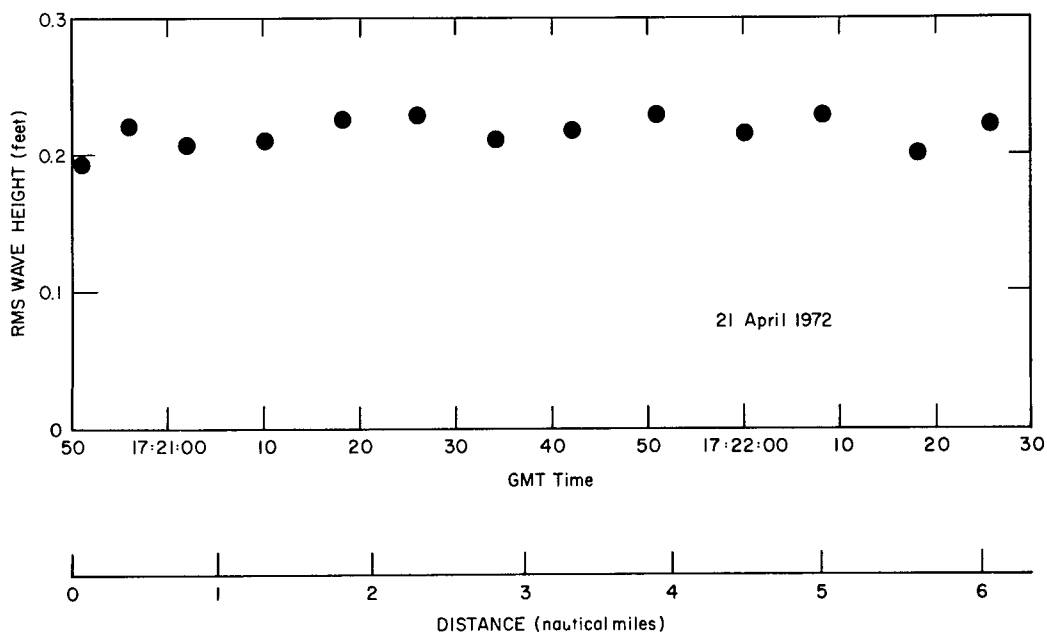


Fig. 12—The inferred rms wave height as a function of time and distance for 21 April 1972

## CONCLUSIONS

The ocean surface descriptors necessary in correlating multipath effects with the roughness of the ocean surface have been determined using Sea Photo Analysis techniques. The techniques applicable to this particular study, the manner in which surface slopes are recorded on film, and optical and computer analysis of the film have been explained. It

has been shown that the Fourier decomposition of the images yield slope spectra. The valid portions of the spectra have been fitted to an equivalent form derived from the Pierson-Moskowitz wave-height spectrum. The empirical equations used to determine rms wave heights and slopes and auxiliary equations for rms slope and wave-height spectra have been given. It has been shown that in the type of analysis used in this study many of the spectral distortions arising from experimental limitations can be avoided.

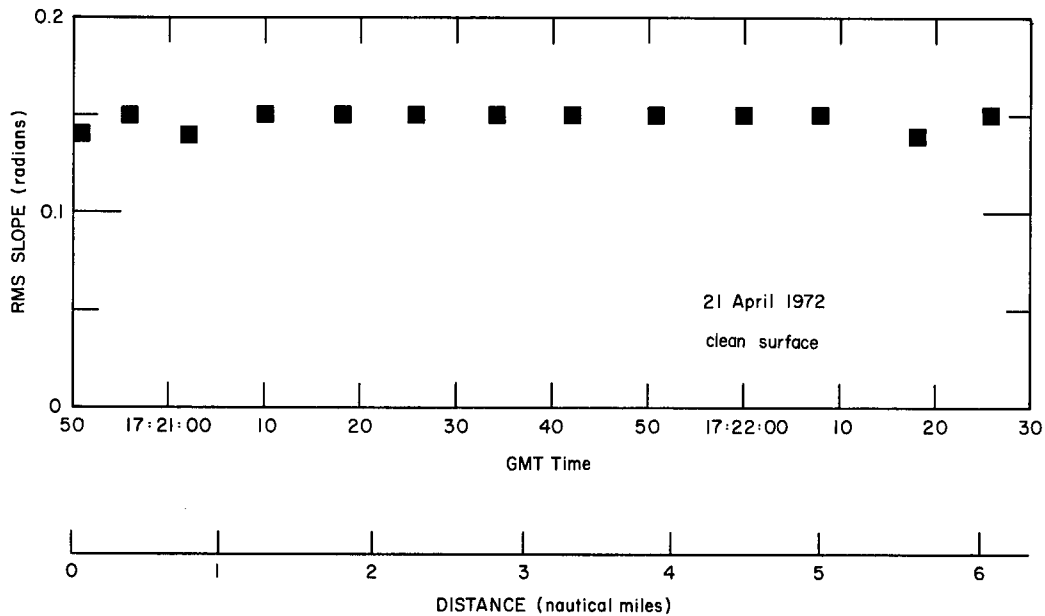


Fig. 13—The inferred rms slope as a function of time and distance for 21 April 1972

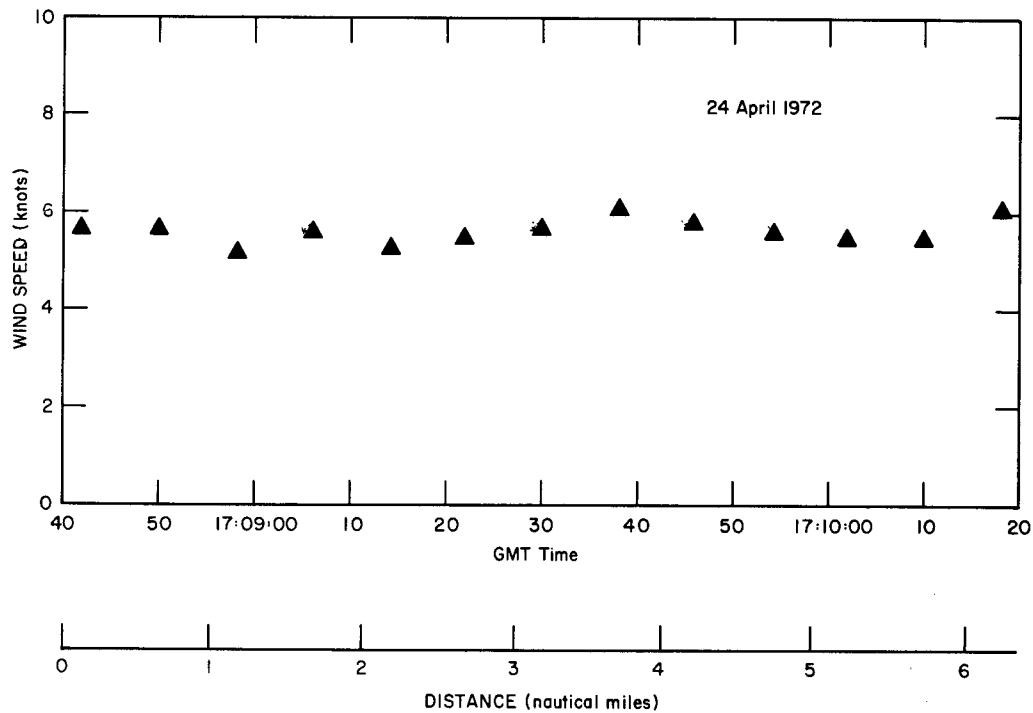


Fig. 14—The inferred wind speed as a function of time and distance for 24 April 1972

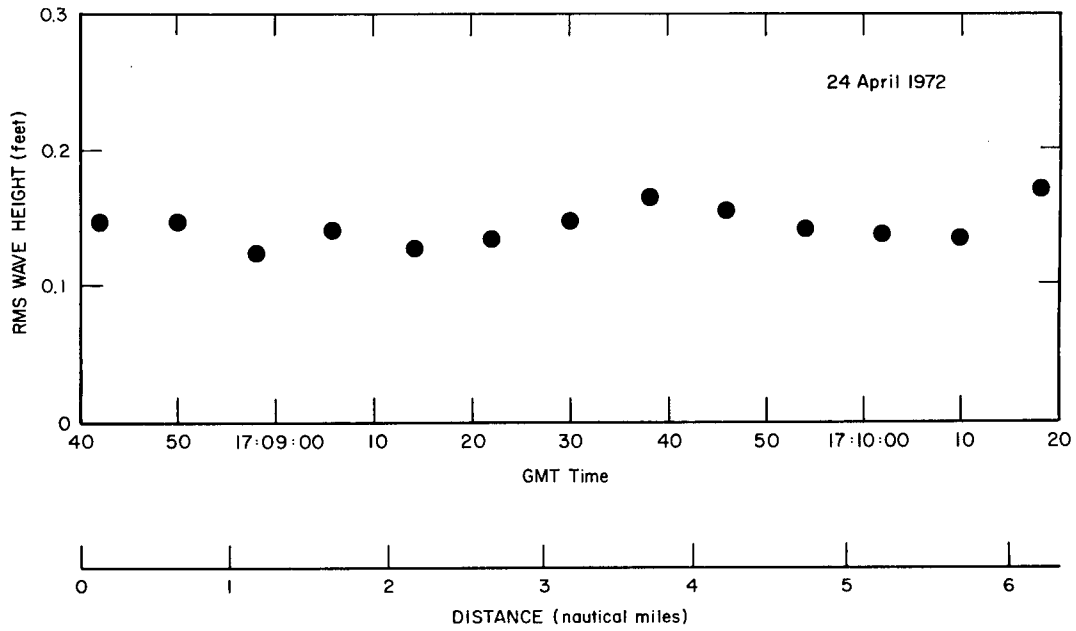


Fig. 15—The inferred rms wave height as a function of time and distance for 24 April 1972

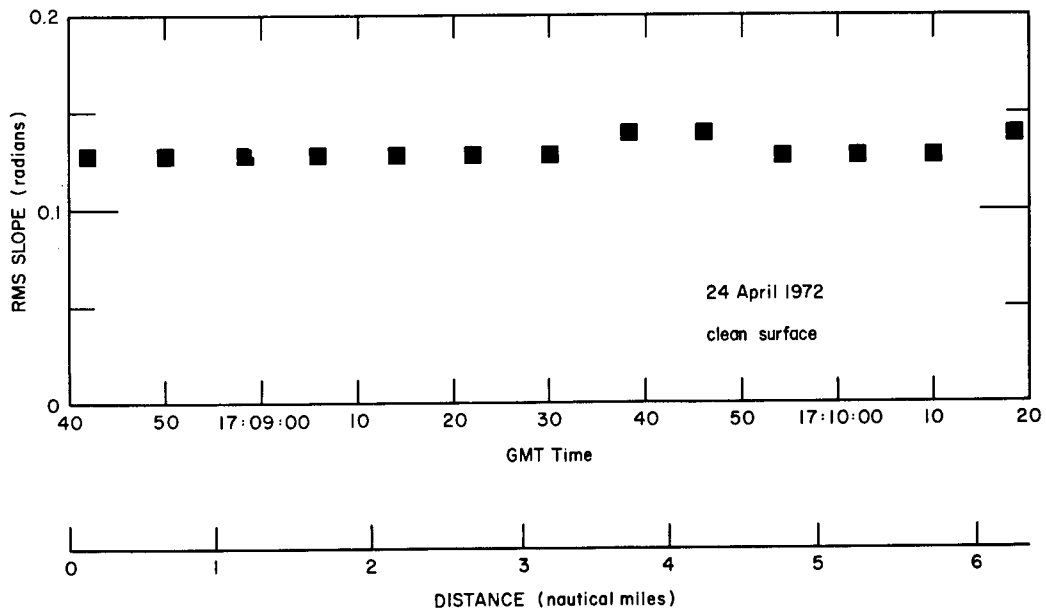


Fig. 16—The inferred rms slope as a function of time and distance for 24 April 1972

Pertinent facts concerning the photographs have been explained and the type of analysis used for each data set has been listed. The time of day, averaged heading of waves, wind speed, rms wave height and rms slope for clean and slick surface, have been determined for each analyzable data set, with minimum, average, and maximum values given for those sets that could be analyzed optically. Root-mean-square slopes due to different water wavelength bands and wave-height spectra may be calculated using the equations given in this report. The parameters inferred from the analysis appear to

describe very well the ocean surface at the time and place at which the photography was taken.

#### ACKNOWLEDGMENTS

The author thanks Messrs. D. Stilwell, Jr., W.C. Keller, and L.I. Moskowitz for their advice and assistance, Mr. J.C. Daley for programming the computer and analyzing the data, and Messrs. O.K. Larison and J.W. Eng for their assistance in the optical and computer analysis of the data.

#### REFERENCES

1. D. Stilwell, Jr., "Directional Energy Spectra of the Sea from Photographs," *J. Geophys. Res.* 74 (No. 8), 1974 (1969)
2. J.W. Goodman, *Introduction to Fourier Optics*, McGraw-Hill, New York, p. 88, 1968
3. W.J. Pierson, Jr., and L. Moskowitz, "A Proposed Spectral Form for Fully Developed Wind Seas Based on the Similarity Theory of S.A. Kitaigorodskii," *J. Geophys. Res.* 69 (No. 24), 5181 (1964)
4. B. Kinsman, *Wind Waves*, Prentice-Hall, Englewood Cliff, p. 389, 1965
5. L. Moskowitz, "Estimates of the Power Spectrums for Fully Developed Seas for Wind Speeds of 20 to 40 Knots," *J. Geophys. Res.* 69, (No. 23), 5161 (1964)
6. C. Cox and W. Munk, *Slopes of the Sea Surface Deduced from Photographs of Sun Glitter*, Bull Scripps Institution of Oceanography, Vol. 6, No. 9, 401-488, University of California Press, Berkeley and Los Angeles, 1956

## APPENDIX

### HINDCAST DATA AND COMPARISON WITH INFERRED DESCRIPTORS

The techniques of Sea Photo Analysis have been used to obtain the required descriptors of the wind-generated seas encountered in this program. The roughness known as sea, however, is but one of the two components of the ocean surface affecting the scattering of electromagnetic energy. The other component is swell. Therefore the Naval Research Laboratory recommended that the Federal Aviation Administration obtain hindcast data on swell. Such data were obtained from the Naval Oceanographic Office and are summarized in Table A1. The data give the direction from which the swell was propagating, the wave height measured from crest to trough, and the period of the swell. The wavelength  $L$  of the swell (assumed to be sinusoidal) may be estimated from [A1]

$$L = 5.12 T^2 , \quad (A1)$$

where  $L$  has the units of feet when the period  $T$  is given in seconds.

Table A1 also includes hindcast data for the sea by the Naval Oceanographic Office (NOO) and for a combined sea and swell by the Canadian Forces Meteorological and Oceanographic Center, Atlantic (CFMOCA). Three differences exist in the manner of reporting the sea (or combined sea and swell) hindcasts and the inferred descriptors given in this report. First, the time and location for which the hindcast is given is not always the same as the time and location at which the aerial photographs were taken. The positions for the hindcasts differ by as much as 250 nautical miles from those at which the photographs were taken. Depending on frontal positions and wind field perturbations in the area, this could account for some of the discrepancy between the hindcast and the inferred data. Second, the hindcasts give the direction from which the wind was blowing, generating (sea) waves heading in the opposite direction. Therefore, the directions given in the sea (or sea and swell) hindcasts differ by 180 degrees from those given in the main text (tables 2 and 3). Third, the hindcasts list a significant wave height,  $H_{1/3}$  (the average of the highest 1/3 of all wave heights measured crest to trough), which is related to the rms wave height given in this report by [A2]

$$H_{1/3} = 4\sigma_h . \quad (A2)$$

The inferred descriptors given in this report are compared to the sea (sea and swell) hindcasts in Table A2. A linear interpolation in time was used to adjust the NOO hindcasts to the time the photographs were taken. The differences in wave headings were determined by adding  $180^\circ$  to the directions given in the hindcasts and then subtracting that value from the Averaged Heading of Waves given in Table 2. The headings given in Table 2 were determined from the photographs and spectra to better than  $\pm 3^\circ$ . Therefore, the differences in wave headings given in Table A2 are mostly errors in the hindcast data (except in those cases where the time and/or location for the hindcast is sufficiently removed from that at which the photographs were taken to be in a different wind field).

Table A1  
Hindcast Wave Information

Date	Site of Experiment (°N, °W)	Time (GMT)	Hindcast by Naval Oceanographic Office						Hindcast by Canadian Forces Meteorological and Oceanographic Center, Atlantic, for Combined Sea and Swell					
			Sea			Swell			Sea			Swell		
			Site (°N, °W)	Time (GMT)	Wind Dir. (deg)	Signif. Wave Height (ft)	Average Period (s)	Dir. (deg)	Wave Height (ft)	Period (s)	Site (°N, °W)	Time (GMT)	Wind Dir. (deg)	Signif. Wave Height (ft)
5-1-71	33.0, 65.0	1812	225	5.1	4.5	135	1.4	6	—	—	—	—	—	
5-24-71	38.5, 62.0	1858	293	16.8	8.2	—	None	—	—	—	—	—	—	
5-25-71	40.0, 57.0	2056	315	14.3	7.5	—	None	—	—	—	—	—	—	
5-26-71	39.5, 59.0	1632	—	None	—	293	8.4	8	—	—	—	—	—	
9-2-71	52.0, 45.0	1921	225	2.6	3.2	293	5.3	9-10	—	—	—	—	—	
9-22-71	40.0, 57.0	1720	225	4.2	4.0	—	None	—	—	—	—	—	—	
10-13-71	41.0, 51.5	1821	225	2.6	3.2	225	5.7	9-10	40.0, 57.0	1630	090	6.6	6	
10-14-71	42.5, 48.5	1827	315	5.9	4.8	315	3.6	6	42.5, 48.5	1630	280	8.2	5	
10-15-71	41.0, 58.0	1924	—	None	—	315	2.8	6-7	40.0, 57.0	1530	280	3.3	8	
3-4-72	38.0, 61.5	1703	135	1.8	2.7	—	None	—	—	—	—	—	—	
3-7-72	40.0, 57.0	1620	113	4.2	4.1	—	None	—	—	—	—	—	—	
3-8-72	41.0, 51.5	1853	225	6.5	5.1	203	9	7	—	—	—	—	—	
4-20-72	44.0, 49.0	1812	248	2.0	2.9	203	11	8	40.0, 57.0	1530	280	11.5	7	
4-21-72	45.0, 53.5	1721	293	6.5	5.1	270	6	6	—	—	—	—	—	
4-22-72	43.5, 59.5	1732	315	2.7	3.2	293	5	10	41.0, 51.5	1530	270	4.9	5	
4-24-72	42.5, 58.5	1709	180	0.5	1.3	—	None	—	—	—	—	—	—	
			270	14.3	7.5	338	18	8-9	42.5, 48.5	1530	310	19.7	10	
			315	3.6	3.8	—	None	—	41.0, 51.5	1530	210	16.4	10	
			315	4.7	4.3	270	6	7-8	—	—	—	—	—	
			315	8.8	5.4	—	None	—	40.0, 57.0	1530	290	11.5	8	
			270	6.6	5.1	293	8	8-9	—	—	—	—	—	
			315	4.7	4.3	203	7	7-8	40.0, 57.0	1530	210	11.5	9	
			293	3.3	3.6	023	6	7-8	—	—	—	—	—	

Table A2  
Comparison of Hindcast Data With Inferred Descriptors

Date	Difference in Wave Heading (deg)		RMS Wave-Height Ratio	
	NRL - NOO	NRL - CFMOCA	NRL/NOO	NRL/CFMOCA
5-1-71	-25	—	0.055	—
5-24-71	+16	—	0.51	—
5-25-71	+41	—	0.50	—
5-26-71	-25	—	0.67	—
9-2-71	+11	—	0.33	—
9-22-71	-88	-03	1.8	0.16
10-13-71	-45	-90	0.82	0.51
10-14-71	—	+35	—	0.43
10-15-71	+90	-60	0.77	0.56
3-4-72	+96	—	2.2	—
3-7-72	+17	+47	1.0	0.96
3-8-72	+68	-60	0.40	0.95
4-20-72	+33	-07	0.26	2.2
4-21-72	-35	+70	0.19	0.078
4-22-72	+19	+03	0.54	0.92
4-24-72	-06	+80	0.17	0.11

The rms wave-height ratio is the inferred rms wave height divided by the hindcasted rms wave height for the sea ( $\frac{1}{4}$  the significant wave height of the sea). The wave heights hindcasted by the Naval Oceanographic Office for swell were subtracted from the hindcasts by the Canadian Forces Meteorological and Oceanographic Center, Atlantic to yield an effective significant wave height for the sea. These effective values were then used to calculate the rms wave-height ratios for the NRL/CFMOCA data. In seven of the comparisons, 1 May 1971 (NOO), 22 September 1971 (CFMOCA), 14 October 1971 (CFMOCA), and 21 and 24 April 1972 (NOO and CFMOCA), visual inspection of the photographs reveals that the hindcasts do not describe the photographed conditions. The effective wind speeds required to generate the significant wave heights hindcasted for these sets may be calculated using Eqs. (A2) and (45). The wind speeds so calculated range from 14 to 25 knots. Since whitecapping begins at wind speeds of about 10 to 12 knots, the photographs for the above sets should show whitecapping. They do not. (The imperfections in the unretouched examples in Fig. 7, such as film scratches and dust spots, should not be confused with whitecapping as shown in Fig. 7b, 7d (very few), 7e, 7g, 7j, 7k, 7m, and 7o.) The effective wind speeds for these sets are therefore less than 12 knots, as indicated by inferred wind speeds in Table 2.

The effective wind speeds required to generate the significant wave heights hindcasted for 2 September 1971 and 20 April 1972 (NOO) are 26 and 28 knots respectively. Therefore, Figs. 7e and 7m should show more whitecapping and spray than Fig. 7b (21.4 knots). Since these figures show significantly less whitecapping and no spray, the hindcasts are not representative of these data sets.

In the remaining comparisons the rms wave-height ratio varies between 0.40 and 2.2. In view of the foregoing, such differences in data taken on site and that hindcasted from

macroscopic pressure systems and wind fields over the open ocean should be considered very good.

- A1. W.J. Pierson, Jr., G. Neumann, and R.W. James, *Practical Methods for Observing and Forecasting Ocean Waves by means of Wave Spectra and Statistics*, Navy Hydrographic Office, Washington, D.C., 1955, H.O. Pub. 603, p. 22.
- A2. M.S. Longuet-Higgins, *J. Marine Res.* 11, 245 (1952), or L. Moskowitz, *J. Geophys. Res.* 69, 5161 (1964).

Security Classification		
<b>DOCUMENT CONTROL DATA - R &amp; D</b> <i>(Security classification of title, body of abstract and indexing annotation must be entered when the overall report is classified)</i>		
1. ORIGINATING ACTIVITY (Corporate author)		2a. REPORT SECURITY CLASSIFICATION
Naval Research Laboratory Washington, D.C. 20375		Unclassified
		2b. GROUP
3. REPORT TITLE		
Determination of Ocean Surface Descriptors Using Sea Photo Analysis Techniques		
4. DESCRIPTIVE NOTES (Type of report and inclusive dates)		
Final report on the first phase of the NRL Problem		
5. AUTHOR(S) (First name, middle initial, last name)		
Roger O. Pilon		
6. REPORT DATE	7a. TOTAL NO. OF PAGES	7b. NO. OF REFS
July 18, 1973	38	8
8a. CONTRACT OR GRANT NO.	9a. ORIGINATOR'S REPORT NUMBER(S)	
NRL Problem R07-20 b. PROJECT NO. FAA DOT-FA71WAI-220 c. d.	NRL Report 7574	
	9b. OTHER REPORT NO(S) (Any other numbers that may be assigned this report)	
10. DISTRIBUTION STATEMENT		
Approved for public release; distribution unlimited.		
11. SUPPLEMENTARY NOTES	12. SPONSORING MILITARY ACTIVITY	
Sponsored by Department of Transportation Federal Aviation Administration Washington, D.C. 20591		
13. ABSTRACT		
<p>The techniques of Sea Photo Analysis have been used to obtain surface truth descriptors of the open ocean from an aircraft. Aerial photographs were taken such that the density fluctuations of the negatives were related to surface slope. The slope spectra, obtained by Fourier analysis of the negatives, were fitted to an equivalent form of the Pierson-Moskowitz wave height spectrum. The photographs, the wave height spectrum, and the rms slope equations determined by Cox and Munk then yielded the averaged heading of the waves, the equivalent wind speed, the rms wave height, and the rms slope for clean and slick surfaces. The optical techniques of Sea Photo Analysis used in this program and digital analysis, used when whitecaps were present in the photographs, are discussed. The empirical equations used to determine rms wave height and slope and auxiliary rms slope and wave height spectrum equations are given. Surface descriptors were inferred for seas driven by winds from 3 to 21 knots occurring on 16 separate days.</p>		

14. KEY WORDS	LINK A		LINK B		LINK C	
	ROLE	WT	ROLE	WT	ROLE	WT
Sea photo analysis (SPA)						
Optical analysis						
Photography						
Computer analysis						
Fourier analysis						
Ocean spectra						
Two-dimensional slope spectra						
Effective wind speed						
Wave height						
Wave slope						